(Published in *CIRP Journal of Manufacturing Science and Technology*, 2021)

Finite Element Modeling of Coating Thickness Using Heat Transfer Method

Yafeng Li[1,2], Anvesh Dhulipalla[1], Jian Zhang[1], Hye-Yeong Park[3], Yeon-Gil Jung[3], Dan Daehyun Koo[4], Jing Zhang[1*]

1. Department of Mechanical Engineering, Indiana University - Purdue University Indianapolis, USA

2. Tianjin Key Laboratory of Modern Mechatronics Equipment Technology, Tiangong University, Tianjin, P.R. China

3. School of Materials Science and Engineering, Changwon National University, Republic of Korea

4. Department of Engineering Technology, Indiana University - Purdue University Indianapolis, USA

*Corresponding author: jz29@iupui.edu; +1-317-278-7186

Abstract

A new heat transfer based finite element model is proposed to simulate coating thickness in the electron-beam physical vapor deposition (EB-PVD) process. The major advantage of the proposed model is that it is much computationally efficient than the traditional ray-tracing based model by about two orders of magnitude. This is because the Gaussian distribution heating source has the same profile as the cosine relation used in the ray-tracing method. Firstly, the model simulates the

temperature profile of a metal substrate heated by a heating source with a Gaussian distribution. Then using a calibrated conversion process, the temperature profile is converted to corresponding coating thickness. The model is successfully demonstrated by three validation cases, including a stationary disk, a stationary cylinder, and a rotary three-pin component. The predicted coating thicknesses in the validation cases are in good agreement with either the ray-tracing based analytical solution or experimental data. After its validation, the model is applied to a rotary turbine blade to predict its coating thickness distribution. In summary, the model is capable to simulate coating thickness in complex shaped parts.

Keywords: Coating; Thickness prediction; Modeling; Heat transfer; Finite element

1. Introduction

Electron beam physical vapor deposition (EB-PVD) is an important evaporation technology to fabricate thermal barrier coatings on superalloy substrates, particularly useful for applications on more harsh conditions, such as turbine blades at high pressures [1]. To understand the coating properties and optimize the process, modeling has been used to simulate the coating process. There are several modeling studies based on the ray-tracing method. Fuke *et al.* developed analytical expressions of coating thickness predictions for simple shape disk and cylindrical surfaces [2]. Schiller *et al.* proposed generic analytical models to predict the coating thickness on simple shaped workpieces, such as plate and cylinder [3]. Pereira *et al.* presented a model that calculates coating thickness considering the shadow effect [4]. Pereira's model is based on the analysis of the vapor deposition flux, and the predicted coating thickness distribution in a three-pin rotatory component is in good agreement with experimental measurement [4].Although the above ray-tracing based method has been widely used, its computational cost is usually prohibitively high, due to calculating individual ray. Therefore, new efficient alternative methods are needed.

In this work, a new heat transfer model is proposed. The motivation is based on the fact that the ray tracing profile in the EB-PVD model, such as presented in Ref. [2], is similar to Gaussian distribution. This work uses Gaussian shaped heating source to emulate the ray-tracing profile, as detailed in Section 2.1. In Ref.[5], the ray tracing algorithm was compared to those obtained with a volumetric heat source in the metal 3D printing simulation. It was found that using ray tracing, the heat input is confined in the proximity of the irradiated surface while volumetric heat sources smear the absorbed energy within the part.

In this work, the objective is to develop a new heat transfer model to simulate coating thickness. The major advantage of the proposed model is that it is much computationally efficient than the traditional ray-tracing based model by about two orders of magnitude. The predicted temperature profile is correlated with coating thickness. The structure of the paper is as follows. Section 2 presents the finite element details with the governing equations. The analogy between the Gaussian distribution and ray-tracing profile is illustrated. The correlation between the temperature profile and coating thickness distribution is presented. Section 3 shows the results of multiple geometries The model is firstly validated using disk and cylinder shaped components, followed by a three-pin component as in Ref. [4]. The validation studies show that the developed model results are in good

agreement with either the analytical model or experimental measurements. Then the model is applied to a gas turbine blade to predict its coating distribution. Section 4 summarizes the results.

2. Finite element model details

2.1 Analogy of Gaussian heat source to ray-tracing profile

In this work, instead of directly computing flux intensity based on the ray tracing method, the heat transfer model is used. The reason is based on the similarity between the Gaussian function shaped heating source and ray intensity predicted by ray racing, as comparatively shown in Figure 1. In the ray racing method, the normalized ray indensity is given by [2]:

$$\frac{I(\alpha)}{I_0} = cos^n\alpha \tag{1}$$

The Gaussian function has the same characteristics as the normal distribution and is defined by [6]:

$$f(x,\sigma,c) = e^{\frac{-(x-c)^2}{2\sigma^2}} \tag{2}$$

where σ is the standard deviation, c is the mean for the Gaussian function, and x is the input value.

From Figure 1, it is evident that there is a similarity between the Gaussian function shaped heating source and ray intensity predicted by ray racing, with corresponding values of n and σ. This similarity allows to use heat transfer to simulate temperature profile, and correlate it with coating thickness.

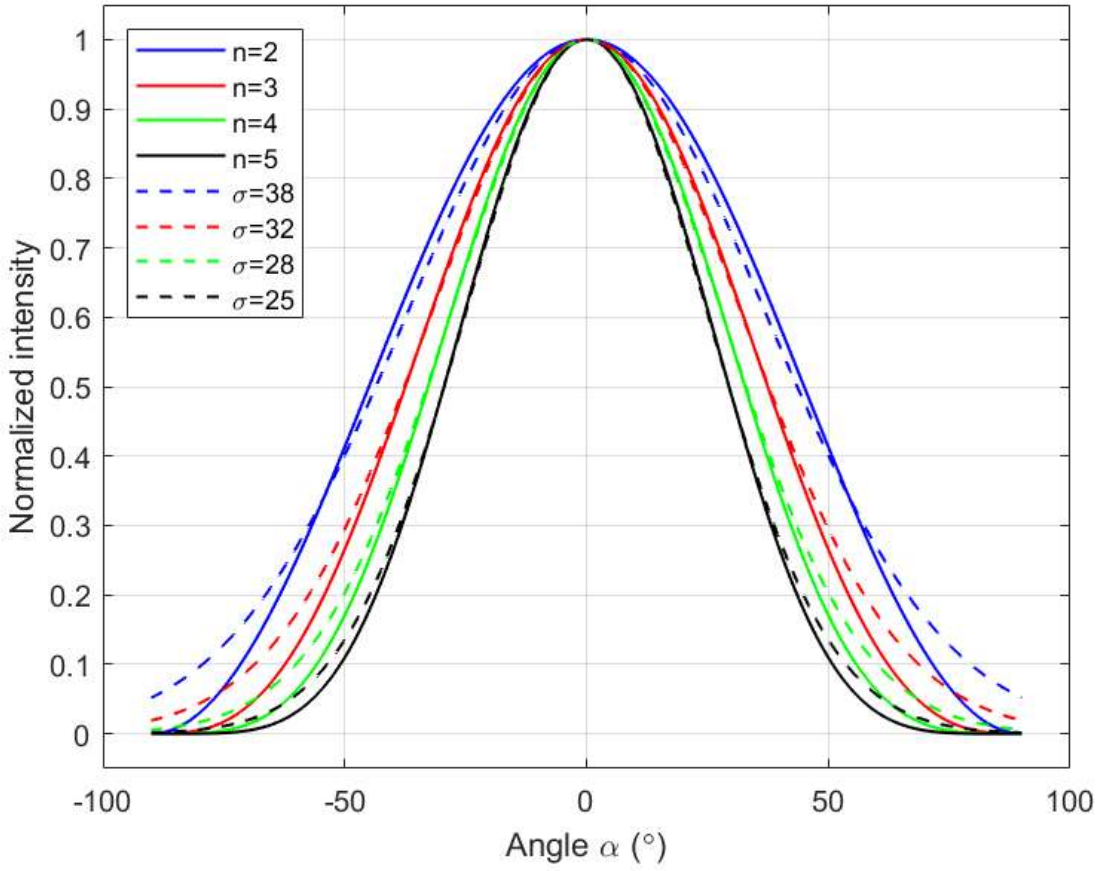

Figure 1: Comparison between Gaussian function of heating source (Equation 2 [6]) used in this study and ray intensity distribution in ray-tracing method (Equation 1 [3]).

For 3D models developed in this work, the 2D coating thickness analytical expressions proposed by Fuke [2] are extended to 3D for disk [7]:

$$d_{sd}/d_{s0} = (1 + \tan^2\alpha_1 + \tan^2\alpha_2)^{-\frac{n+3}{2}} \tag{3}$$

And the normalized 3D thickness for cylinder is [7]:

$$d_{sc}/d_{s0} = (1 - t) \cdot d_1 \cdot d_2 \tag{4}$$

where $d_1 = \frac{1}{(1+\tan^2\alpha_1)^n}$, $d_2 = \left[\frac{h_v^2 \cdot \cos^2\alpha_2}{(h_v+h')^2}\right] \cdot \cos(\alpha_2 + \theta) \cdot \cos^n\alpha_2$, and $t = \sqrt{(h_v \cdot \tan\alpha_1)^2 + \left((h_v + h') \cdot \tan\alpha_2\right)^2}/h_v$

where d_{s0} is the normalizing factor, or the maximum disk coating thickness; α_1 are the divergence angles along the cylinder and transverse directions, respectively, θ is the inclination angle of the tangent to the cylinder at a particular point with respect to. the horizontal direction. Other parameters are the same as those in Ref. [2].

2.2 Correlation between temperature profile and coating thickness distribution

In this heat transfer model, the predicted temperature distribution needs to be correlated with coating thickness. As shown in Figure 2, it is found that there is an excellent linear dependence between the normalized coating thickness and normalized temperature for both the disk and cylinder models, where the normalization process is done by normalizing the thickness and temperature by their maximum values.

It is noted that almost identical slopes in Figure 2 are observed for both the disk and cylinder cases, suggesting the same correlation between the temperature and thickness, irrespective of the component surface curvatures. Additional details of the process are presented in Section 3.1 below.

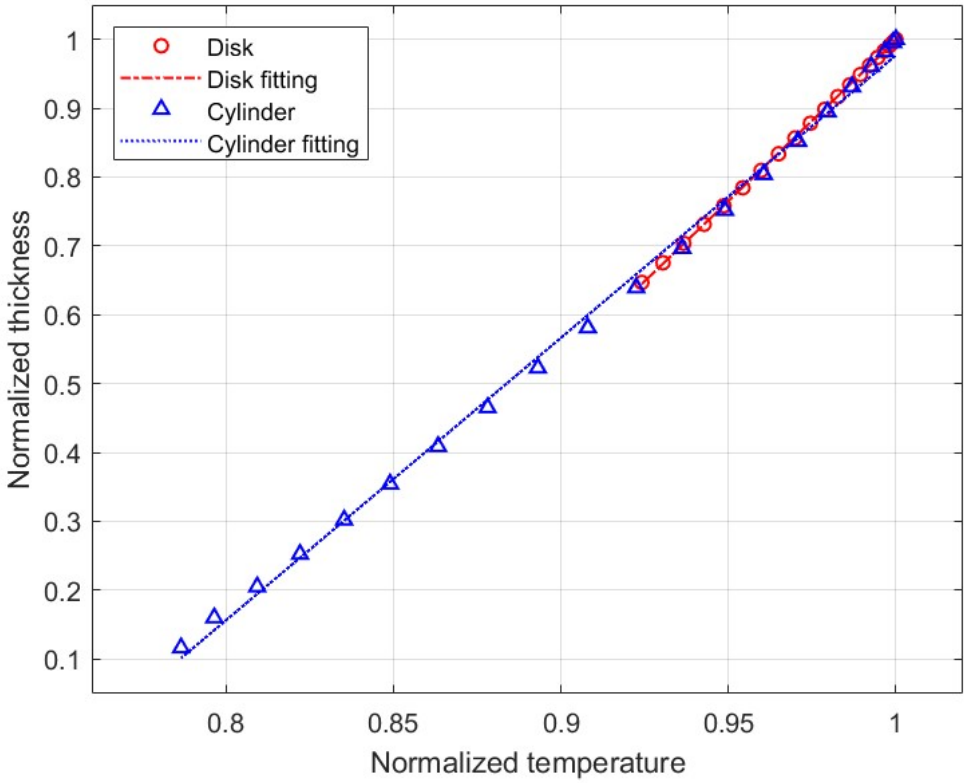

Figure 2: Linear correlations of the normalized coating thickness vs. coating temperature for both the disk and cylinder cases. The fitted lines are also included.

2.3 Governing equations

In this work, a component is heated up by a heating source to simulate the coating process. The incident heat flux from the heating source has a Gaussian distribution on the component's surface, as shown in Figure 1. The transient thermal response of the component and its temperature distribution during the heating process are computed. Then the temperature distribution is converted to the coating thickness using a proposed correlation.

The heat transfer equation to describe temperature distribution is described as[5]:

$$\rho C_p \frac{\partial T}{\partial t} = \nabla[k_{th} \nabla T] + Q \tag{5}$$

where ρ is the material density, C_p the specific heat capacity, T the temperature, t the time, k_{th} the thermal conductivity and Q the heat source in volume due to absorbed heat power.

The heat source term can be written as follows [5]:

$$Q = \varepsilon P_{in}(x,t) \tag{6}$$

where εis the surface emissivity, and P_{in} the incident heat power.

The incident heat power is distributed in time and space with a Gaussian shape[5]:

$$P_{in}(x,t) = P_0 \exp\left\{-\left(\left(\frac{t-t_0}{\tau/2}\right)^2\right)\right\} \exp\left\{-\left(\frac{x}{r}\right)^2\right\} \tag{7}$$

where P_0 is the peak power, t_0 the time shift, τ the pulse time, r the beam radius at half height.

2.4 Geometry and finite element mesh

The disk and cylinder models were built in the finite element package, COMSOL Multiphysics [6]. The dimensions of are 94.2 mm ×15 mm (D×H) for the disk (Figure 3), and 60 mm × 60 mm for the cylinder (Figure 4), so they have the same volume. There are 4,059 3D tetrahedral elements in the disk, and 25,980 elements in the cylinder.

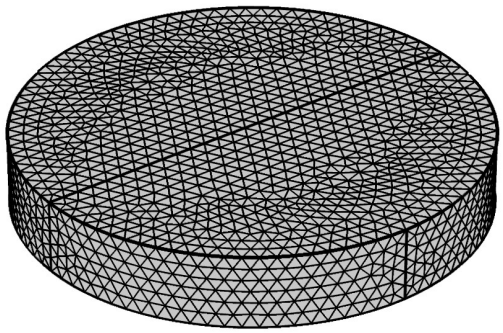

Figure 3: Finite element model of the disk component

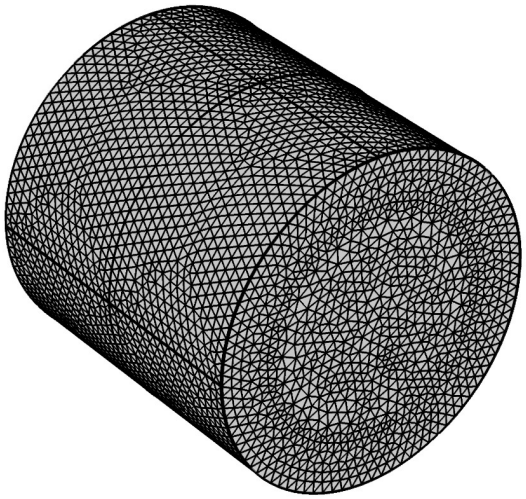

Figure 4: Finite element model of the cylinder component

Figure 5 shows the three-pin model used in Ref. [4]. It is a cluster of three pins mounted on a disk and they are coated in an EB-PVD coater system. The finite element model is reproduced as close as possible as in the reference, since no all dimensions were provided in the reference. In this work, the height of the pins is 100 mm, and their diameter is 8 mm. The pins are equally displaced in a triangle shape, positioned in a circle 15 mm away from the center of the disk and at an angular separation of 120°. The model has 2,848 3D tetrahedral elements.

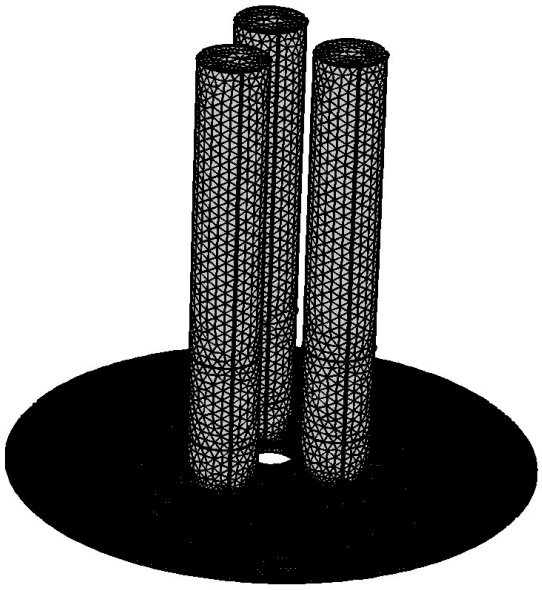

Figure 5: Finite element model of the three-pin component

Figure 6 shows the turbine blade model because of its complexity and industry importance. Turbine blade surface is a complex shape including both convex and concave surface. The height of the model is 3000 μm.

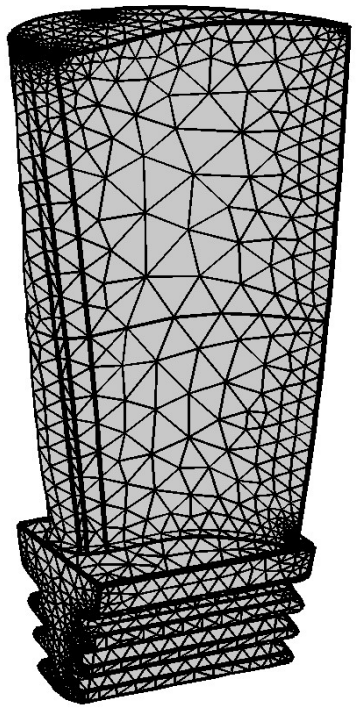

Figure 6: Finite element model of the turbine blade

2.5 Boundary conditions and materials properties

For the disk and cylinder models, the diameter of heating source is π×0.03 m, which covers the whole disk surface and most of the cylindrical surface. The initial temperature is set at 293.15 K. The temperature data are collected along the disk's diameter line and cylinder's half cycle line.

For the three-pin model, same as in Ref. [4], the center of the disk is used as the point of rotation of the three-pin structure. The rotation axis is parallel to the disk's normal. A rotational speed of 20 rpm is used. S1 and S2 are the circular profiles on the pin surface those are 0.03 m and 0.01 m distant from the disk surface, respectively. For the turbine blade model, the component itself is rotated on its stage at an assumed speed of 20 rpm.

For the materials properties, the heat capacity is 385J/(Kg·K), density 8960 Kg⁄m^3, and thermal conductivity 400 W/(m·K).

3. Results and discussion

3.1 Disk and cylinder results

The computed temperature distributions of the disk and cylinders are shown in Figure 7a and Figure 7b, respectively. As shown in the figures, the highest temperature is in the center of the surface.

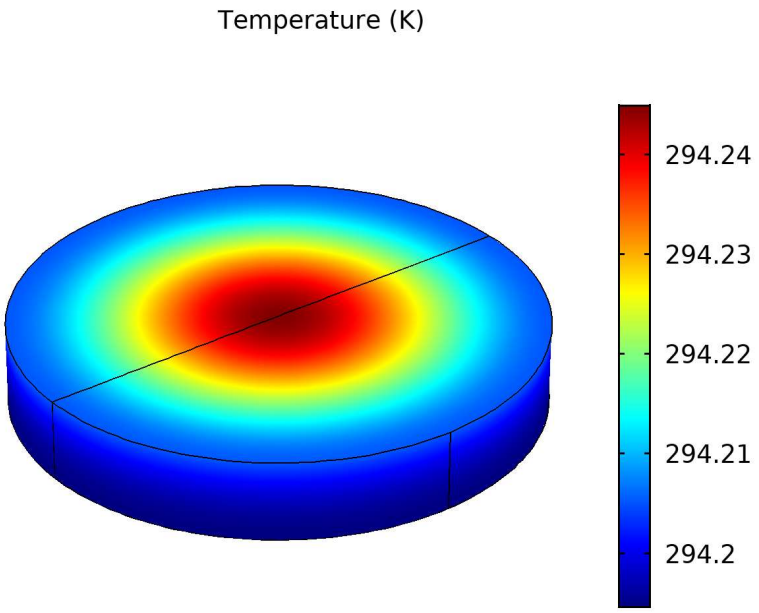

(a)

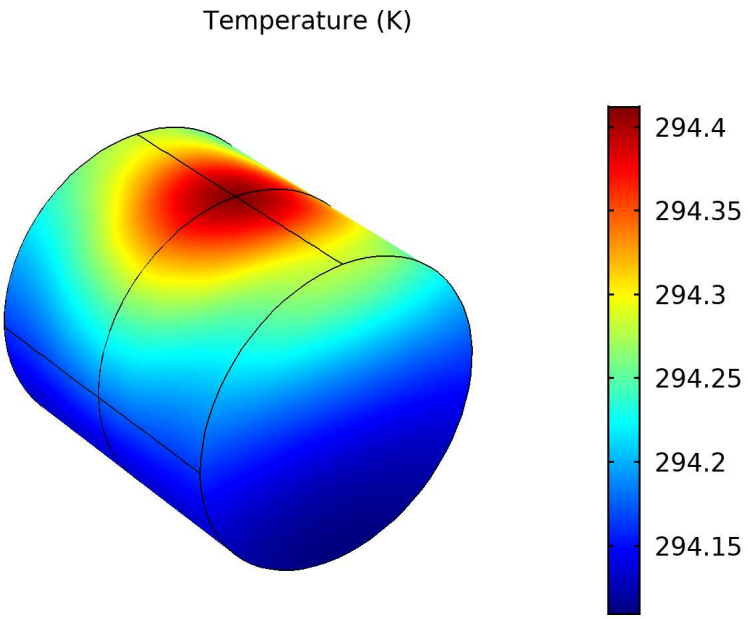

(b)

Figure 7: Temperature distribution of (a) disk, and (b) cylinder.

To view the temperature distribution along particular direction in Figure 7, the temperatures in the diagonal lines of disk and cylinder are plotted in Figure 8. Since both figures show the same characteristics of cubic function, therefore, the relationship between temperature and the angle of divergence from the heating source can be fitted as a cubic polynomial function. The fitted temperature for the disk is[7]:

$$t_{sd} = -7.4979 \times 10^{-10} \cdot \alpha^3 - 6.329 \times 10^{-4} \cdot \alpha^2 + 2.1544 \times 10^{-7} \cdot \alpha + 296.4 \quad (5)$$

Also the fitted temperature profile for the cylinder[7]:

$$t_{sc} = 5.6296 \times 10^{-8} \cdot \alpha^3 - 1.3465 \times 10^{-3} \cdot \alpha^2 - 1.7789 \times 10^{-5} \cdot \alpha + 295.53 \quad (6)$$

where α is the angle of divergence from the ray source.

The temperature distributions are then normalized by their maximum temperatures, so the maximum normalized temperature becomes unity.

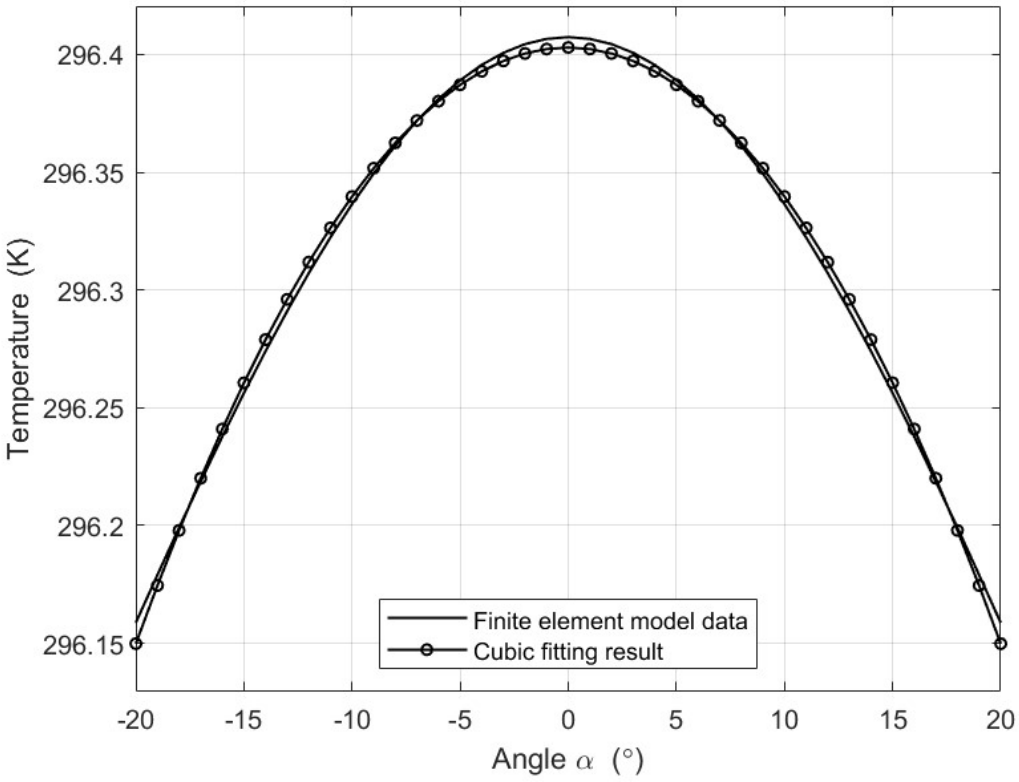
296.4
296.35
296.3
296.25
296.2
296.15
Temperature (K)
-20
-15
-10
-5
0
5
10
15
20
Angle α (°)
Finite element model data
Cubic fitting result

(a)

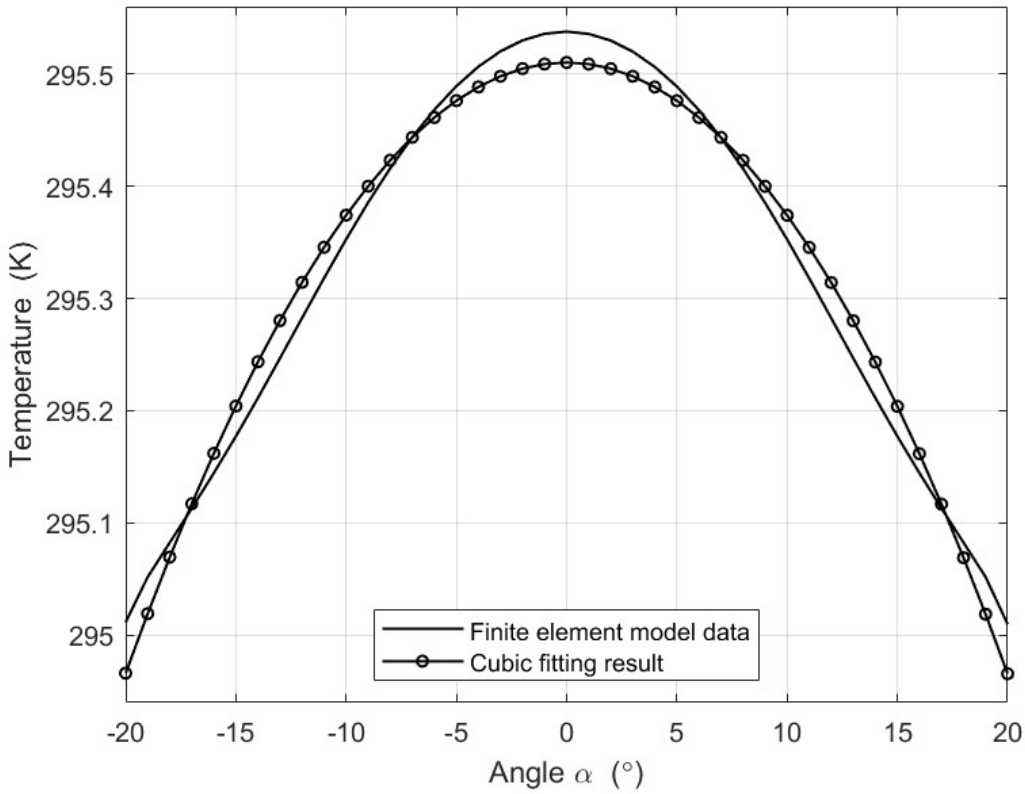

(b)

Figure 8: Predicated temperature distributions along the diagonal direction of (a) the disk, and (b) the cylinder. The fitting curves based on Equations 5 and 6 are also plotted.

By fitting the cubic polynomial with the simulated model data and combining with the analytical models established by Schiller [3], the relation between temperature and coating thickness can be obtained. Simultaneously solving Equations 5 and 7 for disk, and Equations 6 and 8 for cylinder, the relationships between the normalized coating thickness and normalized temperature t_0 can be derived, also as shown in Figure 2:

$$d_{sd}/d_{s0} = (4.6648 \times \text{ to} - 3.6662) \tag{7}$$

$$d_{sc}/d_{s0} = (4.1033 \times \text{to} - 3.1264) \tag{8}$$

Using Equations 7 and 8, the predicted normalized coating thicknesses of the disk and cylinder are shown in Figure 9. As shown in the figure, the components have the maximum coating thickness in the center, and thickness decreases gradually to the sides.

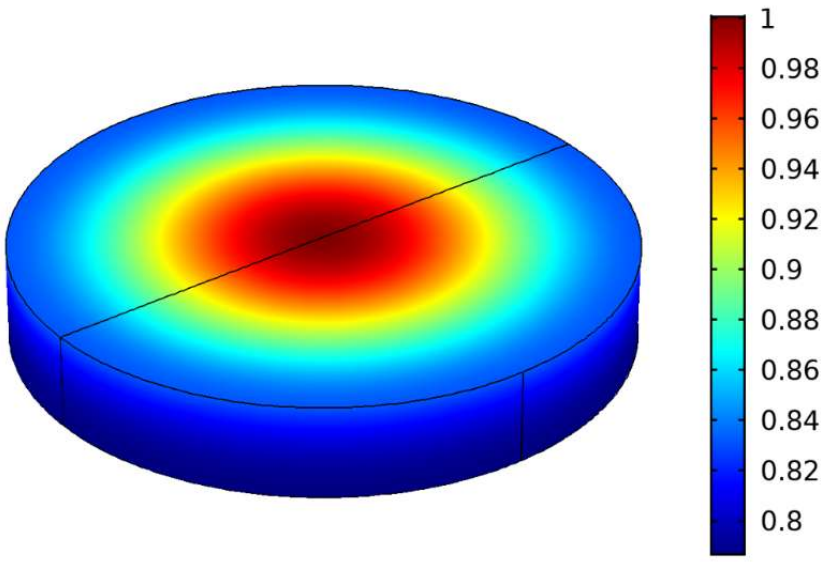

(a)

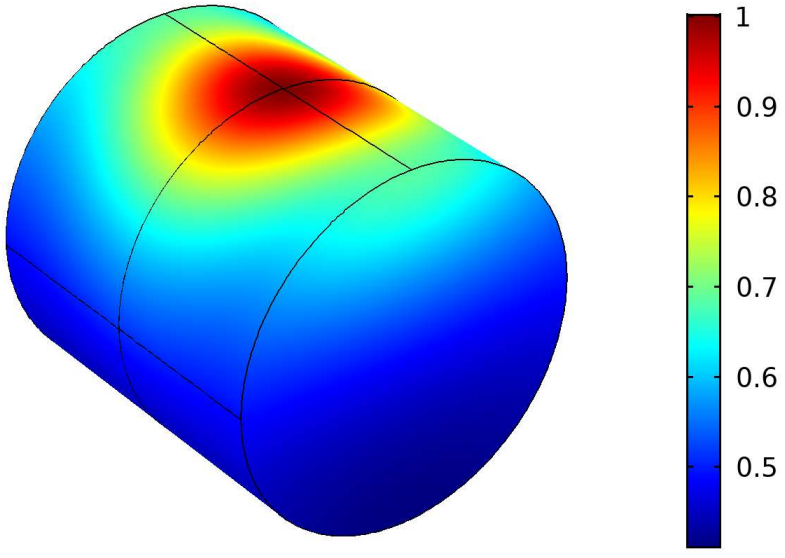

(b)

Figure 9: Predicted normalized coating thickness distributions for (a) disk, (b) cylinder.

To further check correctness of the predicted coating thickness, the comparison between the predicted coating thickness and Ref. [2] is shown in Figure 10. It shows that the predicted thickness are in excellent agreement with Ref.[2].

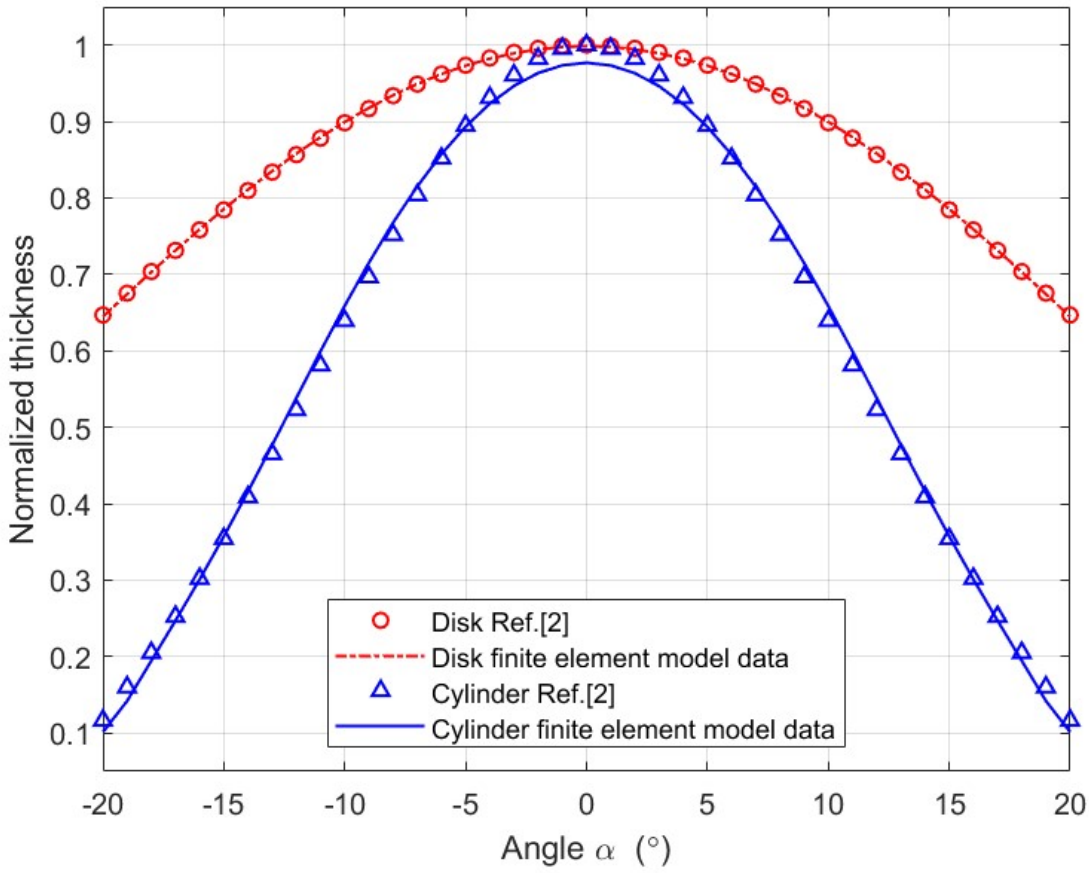

Figure 10: Predicted normalized coating thickness of disk and cylinder, compared with the Ref [2].

3.2 Three-pin component results

The predicted coating thickness in the three-pin component is shown in Figure 11, assuming the maximum coating thickness is 100 μm. For each pin, the center has the maximum thickness, while the thickness decreases away towards ends.

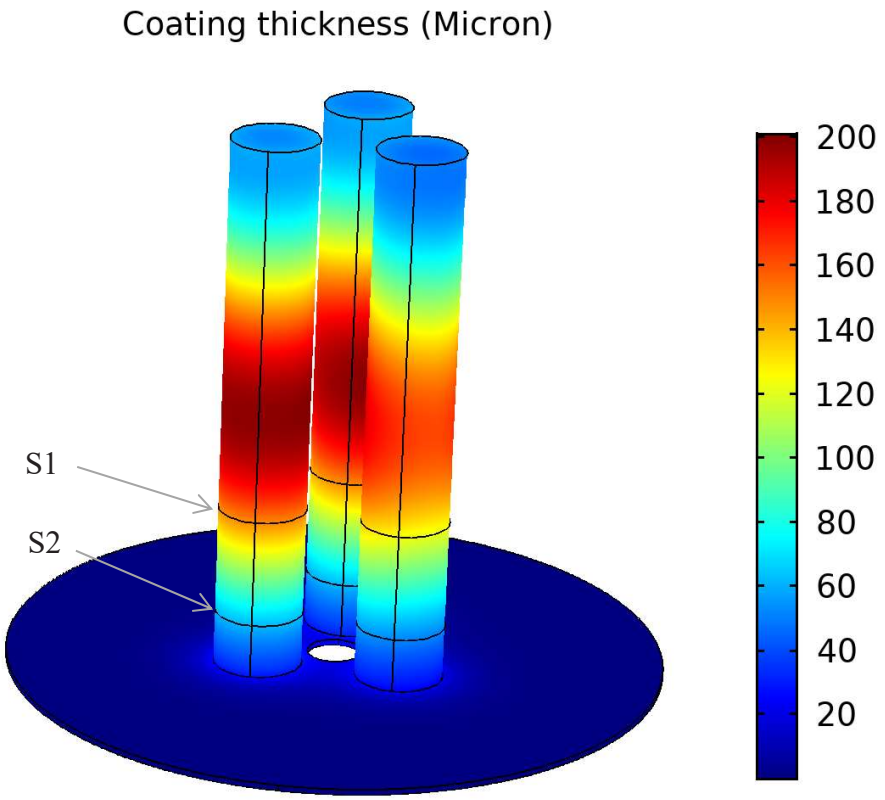

Figure 11: Predicted coating thickness in the three-pin component, assuming the maximum coating thickness is 100 μm.

In order to quantitatively compare with Ref. [4], the coating distributions in the two section planes S1 and S2 are plotted in Figure 12. S1 and S2 are the circular profiles on the pin surface those are 0.03 m and 0.01 m distant from the disk surface. The predictions in this work agree reasonably well with the experimental data in Ref. [4]. The maximum coating thickness occurs at 0 °, and minimal around 150°, which is due to shadowing effect by the other two pins.

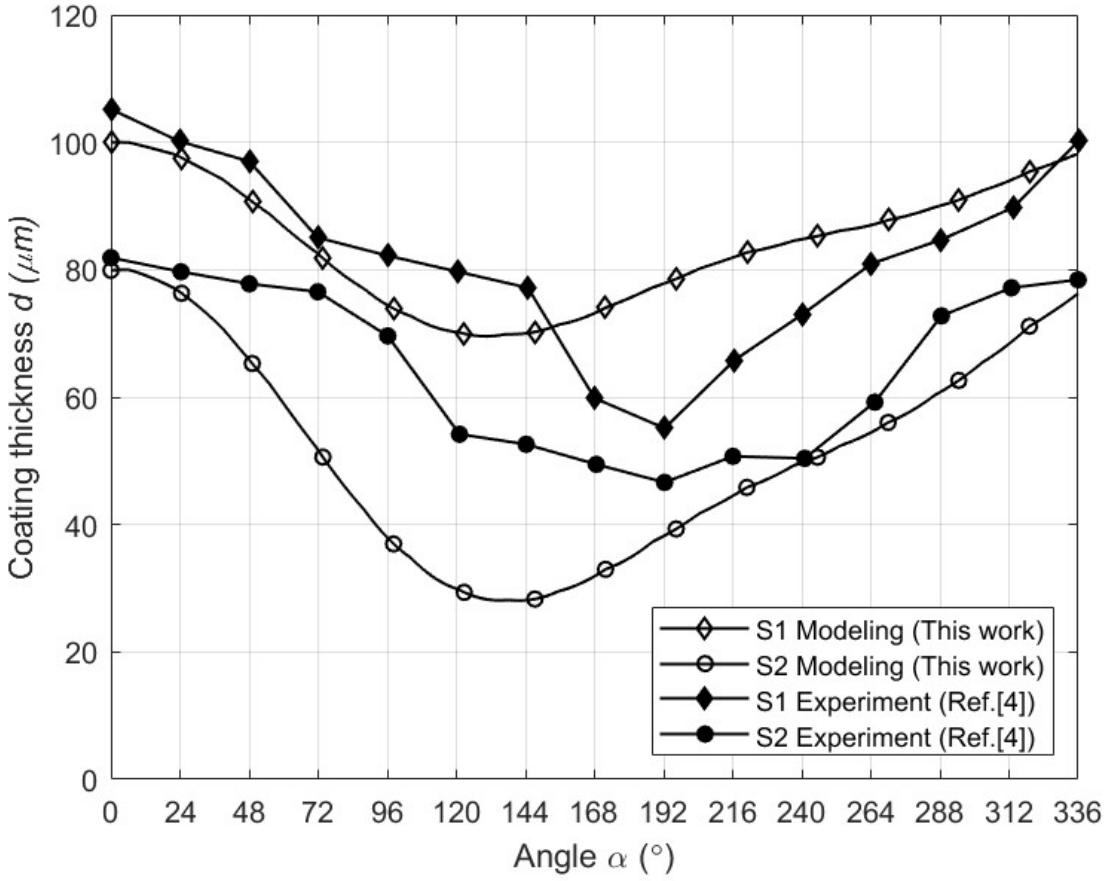

Figure 12: Predicted coating thickness distributions on two cross-sections S1 and S2 of the three-pin model, compared with the experimental points from Ref. [4].

3.3 Turbine blade results

The predicted coating thickness distribution in the turbine blade is shown in Figure 13, assuming the maximum coating thickness is 200 μm. As shown in the figure, the coating thickness of blade trailing edge is higher than that of leading edge. The thickness decreases from the trailing edge to the leading edge, along the pressure side and suction side of the turbine blade.

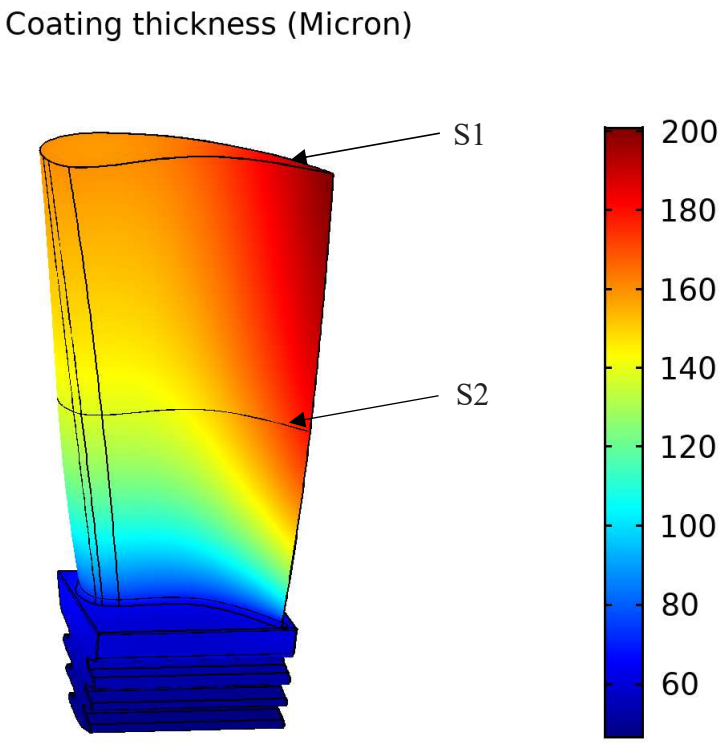

Figure 13: Predicted coating thickness distribution in the gas turbine blade model.

Figure 14 shows the predicted coating distribution along the middle plane section. It shows that trailing edge thickness is the highest. The thickness profiles of pressure side and suction side section are almost symmetrical along the leading edge. The future work would include quantitively comparison with experimentally measured coating thickness distribution using this developed model.

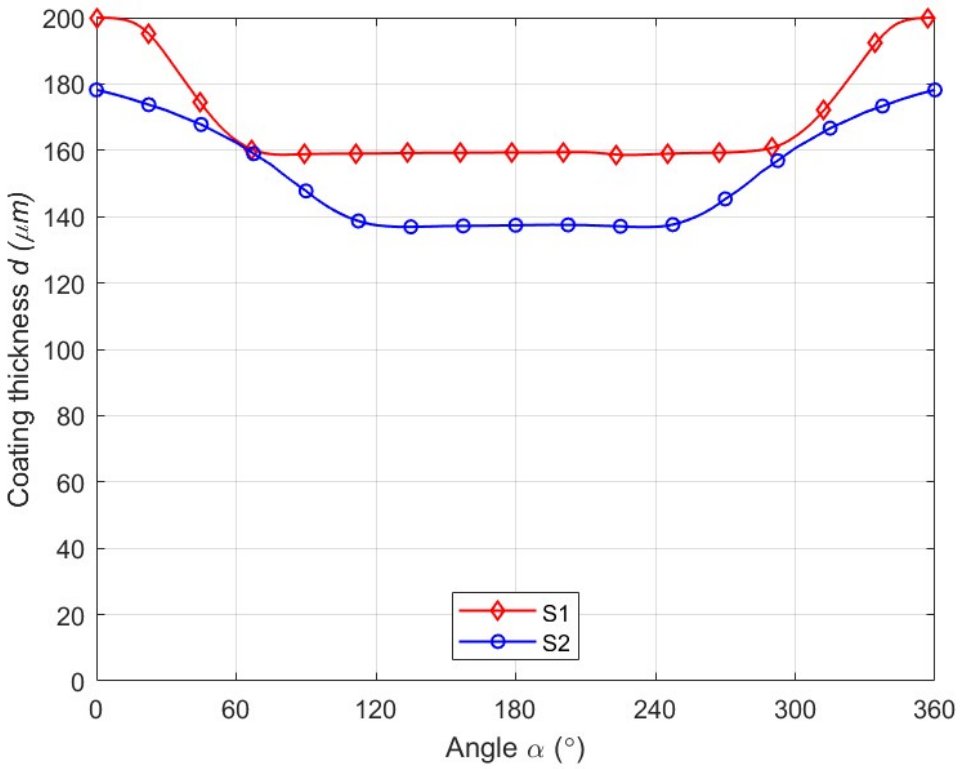

Figure 14: Predicted coating thickness along the central line of the turbine blade.

4. Conclusions

In this work, a heat transfer based finite element model is developed to simulate the coating thickness in the EB-PVD process. The major conclusions are summarized as follows.

1. The developed model is capable to predict coating thickness for workpieces with complex geometries.
2. The model is validated by the disk and cylinder, and the predictions are in excellent agreement with the analytical model based on the ray-tracing method.
3. The coating predications for the rotary three-pin model are also in good agreement with the experimental measurement.

4. The model is applied to the turbine blade model. It shows that trailing edge thickness is the highest. The thickness profiles of pressure side and suction side section are almost symmetrical along the leading edge.

Acknowledgment

Y.F. Li greatly appreciates the support from Tianjin Education Scientific Research Project (2018KJ204) and China Scholarship Council (CSC) Scholarship. This work is partially supported by the “Power Generation & Electricity Delivery (grant number 20181110100310)" of the Korea Institute of Energy Technology Evaluation and Planning (KETEP), granted financial resource from the Ministry of Trade, Industry & Energy (MOTIE), Republic of Korea.

References

1. Peters, M., et al., *EB-PVD Thermal Barrier Coatings for Aeroengines and Gas Turbines.* Advanced Engineering Materials, 2001. **3**(4): p. 193-204.
2. Fuke, I., V. Prabhu, and S. Baek, *Computational Model for Predicting Coating Thickness in Electron Beam Physical Vapor Deposition.* Journal of Manufacturing Processes, 2005. **7**(2): p. 140-152.
3. Schiller, S., U. Heisig, and S. Panzer, *Electron beam technology*. 1982, New York: Wiley.
4. de Matos Loureiro da Silva Pereira, V.E., J.R. Nicholls, and R. Newton, *Modelling the EB-PVD thermal barrier coating process: Component clusters and shadow masks.* Surface and Coatings Technology, 2017. **311**: p. 307-313.
5. Wessels, H., et al., *Investigation of heat source modeling for selective laser melting.* Computational Mechanics, 2019. **63**(5): p. 949-970.
6. *The Heat Transfer Module User's Guide*, COMSOL Multiphysics® v. 5.4. COMSOL AB, Stockholm, Sweden. 2018
7. Li, Y. and J. Zhang, *Private communication.* August 10, 2020.